The WD40 domain of FBXW7 is a poly(ADP-ribose)-binding domain that mediates the early DNA damage response

Qiang Zhang[1], Ahmed S.A. Mady[2], Yuanyuan Ma[3], Caila Ryan[1], Theodore S. Lawrence[1], Zaneta Nikolovska-Coleska[2], Yi Sun[1,4,*,†] and Meredith A. Morgan[1,*,†]

[1]Department of Radiation Oncology, University of Michigan Medical School, Ann Arbor, MI 48109, USA, [2]Department of Pathology, University of Michigan Medical School, Ann Arbor, MI 48109, USA, [3]Shanghai Institute of Precision Medicine, Ninth People's Hospital, Shanghai Jiao Tong University School of Medicine, Shanghai, China and [4]Institute of Translational Medicine, Zhejiang University School of Medicine, Hangzhou 310029, Zhejiang, China

ABSTRACT

FBXW7, a classic tumor suppressor, is a substrate recognition subunit of the Skp1-cullin-F-box (SCF) ubiquitin ligase that targets oncoproteins for ubiquitination and degradation. We recently found that FBXW7 is recruited to DNA damage sites to facilitate nonhomologous end-joining (NHEJ). The detailed underlying molecular mechanism, however, remains elusive. Here we report that the WD40 domain of FBXW7, which is responsible for substrate binding and frequently mutated in human cancers, binds to poly(ADP-ribose) (PAR) immediately following DNA damage and mediates rapid recruitment of FBXW7 to DNA damage sites, whereas ATM-mediated FBXW7 phosphorylation promotes its retention at DNA damage sites. Cancer-associated arginine mutations in the WD40 domain (R465H, R479Q and R505C) abolish both FBXW7 interaction with PAR and recruitment to DNA damage sites, causing inhibition of XRCC4 polyubiquitination and NHEJ. Furthermore, inhibition or silencing of poly(ADP-ribose) polymerase 1 (PARP1) inhibits PAR-mediated recruitment of FBXW7 to the DNA damage sites. Taken together, our study demonstrates that the WD40 domain of FBXW7 is a novel PAR-binding motif that facilitates early recruitment of FBXW7 to DNA damage sites for subsequent NHEJ repair. Abrogation of this ability seen in cancer-derived FBXW7 mutations provides a molecular mechanism for defective DNA repair, eventually leading to genome instability.

INTRODUCTION

Poly(ADP-ribose) (PAR) is a covalent, post-translational modification that enables PARylated-proteins, such as poly(ADP-ribose) polymerase 1 (PARP1) and histones, to recruit many other proteins involved in the DNA damage response to DNA damage sites through non-covalent interactions (1,2). PARP1, the founding member of the PARP family of enzymes, is responsible for the majority of PARylation of cellular proteins for their recruitment to DNA single- and double-strand breaks (SSB and DSB, respectively) to initiate many types of DNA repair, including base excision repair (BER), nucleotide excision repair (NER), and DSB repair (3,4). One critical property of PAR is its highly negative charge conferred by the two phosphate groups of each ADP-ribose subunit, which promote the non-covalent binding of PAR with positively charged PAR binding domains (5). Several PAR-binding domains have been identified in DNA-associated proteins, some of which also function as phospho-Ser/Thr-binding domains such as the FHA and BRCT domains of PNKP and NBS1, respectively (6–10). Proteome-wide analysis of cellular PAR binding proteins has revealed hundreds of potential PAR-associated proteins (11,12), suggesting that other domains with similar features to known PAR-binding domains may also mediate interactions with PAR.

The WD40 domain is an abundant domain in human cells that is well-characterized for its ability to mediate protein-protein interactions. The β-propeller structure of the WD40 domain has multiple binding surfaces that facilitate its versatility in binding diverse substrates including peptide motifs and post-translational modifications (e.g. phospho-Ser/Thr) as well as damaged DNA (13). As a common feature of many WD40 domain-containing E3 ubiquitin ligases, such as CDC20 and β-TrCP, the WD40 domain

plays a critical role in the recognition of cell cycle regulatory protein substrates securin and CDC25A, respectively, for subsequent ubiquitination and proteasomal degradation (14,15). In addition, the WD40 domain has important emerging functions in DNA repair. For example, the WD40 domain of PALB2 mediates interactions with RAD51 and BRCA2 to promote homology directed repair (HDR) (16). Furthermore, the WD40 domain of WRAP53β facilitates interaction between MDC1 and RNF8 to promote DSB repair (17).

In addition to serving as the substrate recognition subunit of many E3 ubiquitin ligases, the WD40 domain also plays important roles in DNA repair (18). For example, the Cullin4^{DDB1} ubiquitin ligase complex specifically binds the DDB2 WD40 domain to form the UV-damaged DNA-binding protein complex, which is essential to global genomic nucleotide excision repair (GG-NER) (19,20). Following DNA damage, the DDB1-DDB2-CUL4A-RBX1 complex catalyzes the non-proteolytic ubiquitination (i.e. K63-linked) of XPC, DDB2, and several histones to facilitate NER. In addition, we recently found that the WD40 domain of FBXW7 within the SCF^{FBXW7} (Skp1-cullin-F-box) complex interacts with phospho-Ser in XRCC4 (Ser 325/326) to promote NHEJ (21). Specifically, upon DNA damage, the nuclear isoform of FBXW7, FBXW7α, is phosphorylated by ATM (Ser 26) and recruited to DNA damage sites, where it catalyzes K63-linked polyubiquitination of XRCC4 and promotes assembly of core NHEJ proteins and NHEJ repair. Independent studies have also demonstrated that FBXW7 functions in other repair pathways, such as interstrand cross-link repair (22,23).

Similar to other characterized PAR binding domains, the WD40 domains of FBXW7 and DDB2 have hydrophobic pockets that recognize negatively charged substrates including phosphodegrons in substrate proteins or damaged DNA, respectively (24–26). Whether the WD40 domain of FBXW7 has PAR binding activity to promote FBXW7 recruitment to DNA damage sites and NHEJ is unknown. Furthermore, the impact of cancer-associated mutations in this domain on recruitment to DNA damage sites and subsequent DNA repair is still unknown. In this study, we reported that the WD40 domains of FBXW7, as well as DDB2, indeed bind with PAR both *in vitro* and *in vivo* whereas the cancer-derived FBXW7 WD40 domain mutants lose the ability to bind PAR, leading to impaired recruitment to DNA damage sites and subsequent defects in DNA repair. Our study provides a detailed molecular mechanism by which PAR recruits FBXW7 to DNA damage sites.

MATERIALS AND METHODS

Plasmids, siRNA, and antibodies

For GFP fusion constructs, FBXW7, FBXW7 ΔWD40, FBXW7 ΔF-box, FBXW7-WD40 (WT and mutants), and DDB2-WD40 were cloned into the pEGFP-C1 vector (Clontech). For GST fusion proteins, FBXW7 ΔWD40, DDB2-WD40, PALB2 WD40 and WRAP53β WD40 were cloned into pGEX-4T-1 vector. For producing purified WD40 domains of FBXW7 and DDB2 for the Biacore assay, DNA encoding the WD40 domains were cloned into pMCSG10 vector. siRNA pools targeting PARP1 and PARP2 were obtained from Dharmacon and transfected into cells using Oligofectamine (Invitrogen) according to the manufacturer's instructions. The antibodies used in this study are anti–β-actin, anti-GST, anti-GFP (Sigma), anti-PARP1 (Cell Signaling), anti-PARP2 (Millipore), anti-PAR (Trevigen), anti-FBXW7 (Bethyl), anti-XRCC4 (BD Transduction Laboratories), anti-phospho-S/TQ (Cell Signaling), and anti-HA (Roche).

Cell culture, cell lysis, immunoprecipitation, and western blotting

MiaPaCa-2 cells were obtained from the American Type Culture Collection (ATCC). HCT116 parental and FBXW7 isogenic cells were gifts from Dr Bert Vogelstein (Johns Hopkins University). HCT116 XRCC4 isogenic cells were purchased from Horizon Discovery. AT fibroblast cells (with and without ATM-reconstitution) were gifts from Dr Mukesh Nyati (University of Michigan). Cells were cultured in Dulbecco's modified Eagle medium (DMEM) supplemented with 10% FBS, 2 mM glutamine and antibiotics. Cells were lysed with RIPA or NETN buffer containing protease and phosphatase inhibitors (Roche). Immunoprecipitation and western blotting were performed following standard protocol as described previously (21).

GST fusion protein expression and pull-down assay

For *in vitro* PAR binding dot blot assays, GST fusion proteins (GST-FBXW7-WD40, GST-DDB2-WD40, GST-PALB2 WD40 and GST-WRAP53β WD40) were expressed in *Escherichia coli* DH5α and purified by using standard procedures. Purified GST fusion proteins (1 pmol) were incubated with biotin-labeled PAR (5 pmol) and streptavidin beads for 2 h at 4°C. After washing with NETN-100 buffer four times, samples were boiled in SDS-sample buffer and elutes were analyzed by western blot with anti-GST antibody. For purification of the WD40 domains of FBXW7 and DDB2, DNA encoding the WD40 domains were cloned into pMCSG10 vector for bacterial expression with an N-terminal His and GST tags and a tobacco etch virus (TEV) cleavage site between the GST- and WD40-coding regions (27). Both plasmids were transformed into Rosetta 2 *Escherichia coli* cells. Bacteria were grown in LB broth at 37°C until OD_{600} reached 0.8. Cultures then were induced with 0.5 mM isopropylthio-β-galactoside and allowed to grow at 16°C overnight together with 1% D-glucose. The cells were harvested by centrifugation (5000 × g, 10 min, 4°C). The cell pellets were resuspended and sonicated in lysis buffer (25 mM HEPES (pH 7.5), 200 mM NaCl, 1 mM DTT, protease inhibitors aprotinin and leupeptin). The proteins were resuspended in lysis buffer with the addition of 10 mM imidazole and purified using Ni-NTA resin, respectively. After first purification, the affinity tag was removed by recombinant His-TEV protease in a dialysis buffer containing 25 mM HEPES (pH 7.5), 150 mM NaCl, 1 mM DTT and 1 mg/ml TEV. For the second step of purification, the cleaved WD40 domain proteins were collected in the flow through fractions after loading on another Ni-NTA resin. Then a further purification was performed by using gel-filtration

chromatography on a Superdex-200 column (GE Healthcare).

PAR binding assays

Approximately 1 μM of each recombinant protein was incubated with 10 μM PAR, 30 μl glutathione agarose in the NETN-100 buffer containing 0.5% NP-40, 50 mM Tris–HCl pH 8.0, 100 mM NaCl, 0.5 mM EDTA with protease inhibitors (Roche). After incubation for 2 h at 4°C, the beads were extensively washed with NETN-100 solution, and bound proteins were released by adding 30 μl sample buffer (150 mM Tris–HCl, 10% SDS, 10 mM EDTA) followed by heating at 95°C for 10 min. Aliquots (1 μl) of samples were dot blotted onto nitrocellulose membranes. After incubation for 30 min at 60°C, membranes were subjected to western blot analysis with anti-PAR antibodies.

Bio-layer interferometry (BLI) binding assay

Biotinylated poly ADP-ribose (PAR) polymer was purchased from Trevigen (Cat. 4336-100-02). BLI experiments were performed using an OctetRED96 instrument (PALL/ForteBio). All assays were run at 30°C using phosphate buffered saline (PBS) from Gibco (10010-023) with continuous 1000 rpm shaking. Super streptavidin (SSA) biosensors were pre-wetted with PBS for 10 min. Biotinylated PAR was immobilized on SSA biosensors by dipping sensors in 0.13 μM solution to reach saturation at around 0.3 nM. Biotinylated blocked streptavidin sensors were used as control sensors prepared by the protocol provided from the manufacturer. PAR loaded sensors were dipped in a serial dilution of FBXW7 WD40 and DDB2 WD40 proteins from 1 to 40 nM and allowed to associate for 3 min and dissociate for 10 min. CHFR was used as a positive control; CHFR binding affinity was determined using the same protocol as for FBXW7 and DDB2, tested in concentrations from 10 to 200 nM. Buffer only reference was included in all assays. Collected raw kinetic data were processed in the Data Analysis software provided by ForteBio using double referencing for binding analysis in which both buffer only sensors and control sensors were subtracted. Resulting binding kinetics were fitted to a biphasic 2:1 heterogeneous binding model from which steady state KD values were calculated.

Irradiation

Irradiations were performed using a Philips RT250 (Kimtron Medical) at a dose rate of ∼2 Gy/min in the University of Michigan, Rogel Cancer Center Experimental Irradiation Shared Resource. Dosimetry was performed using an ionization chamber connected to an electrometer system that is directly traceable to a National Institute of Standards and Technology calibration.

Dot blot

For detecting the interaction of FBXW7 and PAR *in vivo*, MiaPaCa-2 cells were collected after 2 min upon radiation. Cells were lysed in NETN-100 buffer, and the lysates were applied to immunoprecipitation by using anti-FBXW7 (Bethyl) or anti-PAR (Trevigen) antibodies. The immunoprecipitates were extensively washed and spotted onto a nitrocellulose membrane. After air drying, the membrane was blocked with 0.15 M NaCl, 0.01 M Tris–HCl, pH 7.4, 0.1% Tween 20 supplemented with 5% milk and extensively washed with the same buffer. The membrane was probed with anti-FBXW7 or anti-PAR antibody.

Laser microirradiation and imaging of cells

MiaPaCa-2 and HCT116 cells with or without transfection of indicated plasmids were plated on glass-bottomed culture dishes (Mat Tek). Laser microirradiation was performed by using an IX 71 microscope (Olympus) coupled with the MicroPoint Laser Illumination and Ablation System (Andor). A 337-nm laser diode (3.4 mW) transmits through a specific dye cell and then yields a 365-nm wavelength (UVA) laser beam that is focused through a ×60 UPlanSApo/1.35 oil objective to yield a spot size of 0.5–1 μm. Cells were exposed to the laser beam for ∼3.5 ns. The pulse energy is 170 μJ at 10 Hz. Images were taken by the same microscope with CellSens software (Olympus).

NHEJ linearized plasmid assay

pEYFP-N1 (Clontech Laboratories) plasmid was linearized by digestion between the promoter and coding sequence of EYFP with restriction endonuclease NheI. The linear products were purified from agarose gels and transfected into serum-starved (overnight) HCT116 isogenic cells carrying WT or mutant FBXW7. After 12 hr, the cells were harvested and lysed to isolate transfected plasmids by using Plasmid Miniprep Kit (Qiagen). The efficiency of end joining repair was assessed by qPCR of the ligated EYFP region, normalized to an uncut flanking DNA sequence. Primers for qPCR: 5′-GCTGGTTTAGTGAACCGTCAG-3′, 5′-GCTGAACTTGTGGCCG TTTA-3′ (end-joining region); 5′-TACATCAATGGGCGTGGATA-3′, 5′-AAGTCCCG TT GATTTTGGTG-3′ (control).

Comet assays

Single-cell gel electrophoretic comet assays were performed under neutral conditions according to the previous report (28). Briefly, HCT116 FBXW7 isogenic cells (vector control, WT, R465H, or R479Q) were irradiated (5 Gy) and recovered in normal culture medium for indicated time at 37°C. Cells were collected and rinsed twice with ice-cold PBS solution; 2×10^4 cells/ml were combined with 1% LM Agarose at 40°C at a ratio of 1:3 (vol/vol) and immediately pipetted onto slides. For cellular lysis, the slides were immersed in neutral lysis solution (2% sarkosyl, 0.5M Na_2EDTA, 0.5 mg/ml proteinase K, pH 8.0) overnight at 37°C in the dark, followed by washing in the rinse buffer (90 mM Tris buffer, 90 mM boric acid, 2mM Na_2EDTA, pH 8.5) for 30 min with two repeats. Then, the slides were subjected to electrophoresis at 20 V (0.6 V/cm) for 30 min and stained in 2.5 μg/ml propidium iodide for 20 min. All images were taken with a fluorescence microscope and analyzed by Comet Assay IV software (Perceptive Instruments).

Statistics

Statistically significant differences for comet assays were determined by one-way ANOVA with the Tukey post-comparison test in GraphPad PRISM version 7 (Graph-Pad). For laser microirradiaiton, γH2AX and NHEJ assays, a Student's two-tailed *t* test was performed in Graph-Pad PRISM.

RESULTS

The WD40 domains of FBXW7 and DDB2 bind to PAR *in vitro*

We recently reported that FBXW7 rapidly localizes to DNA damage sites to facilitate NHEJ (21). As the WD40 domain of FBXW7 is a well-known phospho-peptide binding domain, we hypothesized that the WD40 domain of FBXW7 and potentially other DNA repair proteins including WRAP53β, DDB2 and PALB2 (16,17,29) might be capable of binding PAR at DNA damage sites. To examine whether the WD40 domain of DNA repair proteins binds PAR, purified recombinant WD40 domains of FBXW7, WRAP53β, DDB2 and PALB2 were incubated with PAR in an *in vitro* binding assay using the previously established PAR binding protein Checkpoint with forkhead-associated and RING domains (CHFR) as a positive control (30). We found that the WD40 domains of FBXW7 and DDB2 bound PAR while those of WRAP53β and PALB2 did not (Figure 1A). These findings were further confirmed in a reciprocal pull-down assay where PAR bound the purified WD40 domains of FBXW7 and DDB2, but not those of WRAP53β or PALB2 (Figure 1B). Furthermore, the WD40 domains of both FBXW7 and DDB2 show positive charge under physiological conditions (theoretical isoelectric points: 8.25 and 9.66, respectively) in Compute pI/MW ExPASy analysis, that is much higher than that of WRAP53β and PALB2 proteins (Supplementary Figure S1A), supporting the potential of electrostatic interactions with PAR.

We further determined the binding affinities of the WD40 domains of FBXW7 and DDB2 to PAR using Bio-Layer Interferometry (BLI). Biotinylated PAR was immobilized on streptavidin sensors that were placed in analyte solutions of FBXW7 WD40, DDB2 WD40, or CHFR to characterize the kinetics and affinity of interaction. As previously reported, CHFR demonstrated high-affinity binding to the immobilized biotin-labeled PAR ($KD = 5.1 \pm 0.1$ nM) (Figure 1C) (31). We found that the WD40 domain of FBXW7 directly bound PAR with high affinity ($KD = 1.8 \pm 0.6$ nM), validating the results of the pull-down assays (Figure 1D, Supplementary Figure S1B). Furthermore, the same domain in DDB2 bound PAR with similar affinity ($KD = 1.4 \pm 0.6$ nM), indicating the importance of the WD40 domain in mediating binding to PAR (Figure 1E and Supplementary Figure S1C). Although an interaction between the WD40 domain of DDB2 and PAR has not been previously described, interactions between DDB2 and PAR, as well as PARP1, are established (32,33). Therefore, to further characterize the interactions between the WD40 domain and PAR, and its significance, the present study is focused on

the novel interaction between the FBXW7 WD40 domain and PAR.

The WD40 domain of FBXW7 binds to PAR in vivo in response to radiation-induced DNA damage

We next assessed the interaction between FBXW7 and PAR *in vivo*. Cells were treated with or without radiation followed by immunoprecipitation of FBXW7 or PAR. The interaction between endogenous FBXW7 and PAR was significantly enhanced by radiation as assessed by both dot blot and western blot (Figure 2A, Supplementary Figure S2A), an effect likely due to the increased PAR synthesis in response to radiation (34), and consistent with the localization of FBXW7 to sites of radiation-induced DSBs (21). This radiation-enhanced interaction was also observed between ectopically expressed HA-FBXW7 and PAR (Supplementary Figure S2B). Reciprocal immunoprecipitation using anti-PAR antibody further confirmed the association of FBXW7 and PAR in response to radiation (Figure 2B). In addition to radiation-induced DNA damage, PAR synthesis occurs in response to agents that induce other types of DNA damage and replication stress (3). To examine whether the interaction of FBXW7 and PAR is increased by other DNA damaging agents, we treated cells with methyl methanesulfonate (MMS), hydroxyurea (HU), or hydrogen peroxide (H_2O_2), agents that produce DNA alkylation, replication stress, or SSBs, respectively. Binding of PAR and FBXW7 was increased in response to all DNA damaging treatment conditions including IR, MMS, and H_2O_2, but was only marginally affected by HU treatment, suggesting that FBXW7/PAR binding is mainly induced by DNA damage (Figure 2C). Finally, to confirm that the WD40 domains of FBXW7 mediate its PAR binding, we made a truncation mutant of FBXW7, containing only the N-terminal domain (ΔWD40) (Figure 2D). We found that the FBXW7 WD40 domain fragment and full length FBXW7 pulled down PAR at a comparable level, while the N-terminal fragment of FBXW7 did not (Figure 2E, F). Similarly, the interaction between the WD40 domain of DDB2 and PAR was comparable to that of full length DDB2 (Supplementary Figure S2C). Thus, in line with the *in vitro* binding data, the WD40 domain of FBXW7 and DDB2 mediates the interaction with PAR *in vivo*, which is enhanced by radiation.

Mutational hotspots in the FBXW7 WD40 domains disrupt PAR binding

We next determined whether cancer-derived mutations in the FBXW7 WD40 domains would abrogate the PAR binding. We focused on R465H and R479Q mutants in the third WD40 repeat of FBXW7 WD40 domain (Supplementary Figure S3A), based on their high frequency in human cancers as well as their loss-of-function in substrate binding activity (35,36). In contrast to wild type FBXW7, neither R465H nor R479Q mutant was found to interact with PAR *in vitro* (Figure 3A). We further analyzed the effect of these mutations on the interaction between full length FBXW7 and PAR in response to radiation-induced DNA damage. While wild type FBXW7 efficiently bound PAR, binding
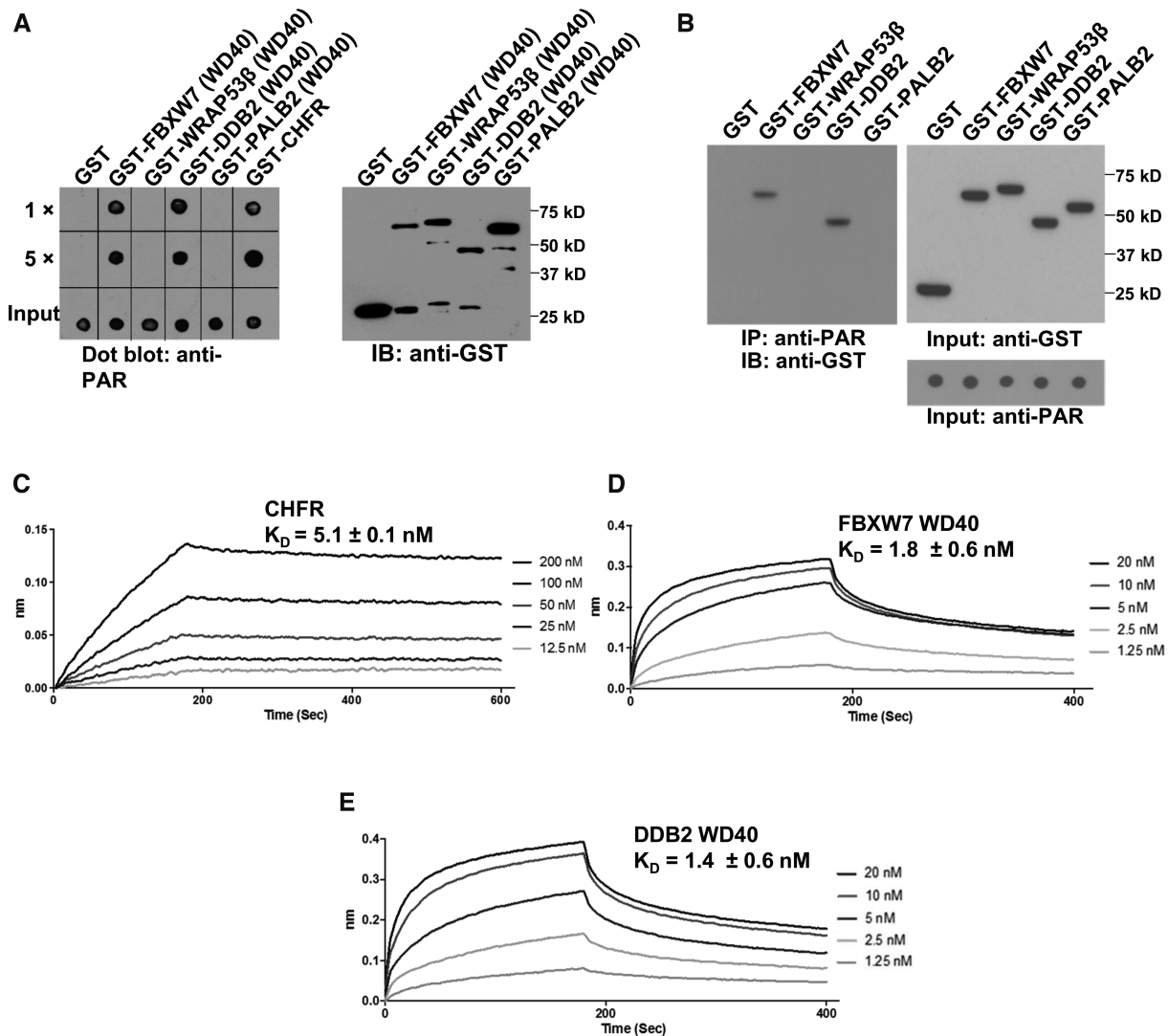
Figure 1. The WD40 domains of FBXW7 and DDB2 bind poly(ADP-ribose). (**A**) The WD40 domains of FBXW7 and DDB2 interact with PAR. GST fusion DNA repair proteins containing WD40 domains were incubated with PAR. The interaction was examined by glutathione agarose bead pull-down and dot blotting with anti-PAR antibody. GST-CHFR was used as the positive control. (**B**) The interactions between PAR and GST fusion recombinant proteins were examined by pull-down with anti-PAR (10H) conjugated beads and blotted with anti-GST antibody. (**C**) Binding affinity of the positive control CHFR with biotin-labeled PAR. (**D** and **E**) The binding affinities between FBXW7 and DDB2, through their homologous WD40 domain, to immobilized biotin-labeled PAR and measured by BLI.

was completely abrogated in the FBXW7 WD40 domain mutants (Figure 3B). The reciprocal IP confirmed that the interaction between FBXW7 and PAR was abolished by these two arginine mutations both in the presence and absence of radiation treatment (Figure 3C). In addition, the 4th repeat of the WD40 domain of FBXW7 contains a highly conserved arginine residue (R505) that is also mutated in cancers. In line with the R465H and R479Q mutants, mutation of arginine at 505 to cysteine also abrogated the interaction of FBXW7 WD40 domain with PAR in vitro (Supplementary Figure S3B).

We further used computational-based modeling to provide a structural basis for the disruption of the interaction between FBXW7 mutants with PAR. Modeling of the FBXW7 WD40 domain interaction with *iso*-ADP-ribose,

based on the known interaction between FBXW7 WD40 and the CyclinE phospho-peptide, revealed complementary electrostatic potential between the positively charged binding sites and negatively charged *iso*-ADP-ribose (Supplementary Figure S3C, D). The residues R465 and R479, as well as R505, play a key role in stabilization of the *iso*-ADP-ribose, likely through salt bridge interactions between guanidinium groups and phosphate moieties (Figure 3D). Thus, arginine residue mutation to other amino acids likely abrogates this stabilization. Taken together, these results provide biochemical and structural evidence of the binding between the FBXW7 WD40 domain and PAR, which is dependent on arginine residues, but disrupted in cancer derived FBXW7 mutants.
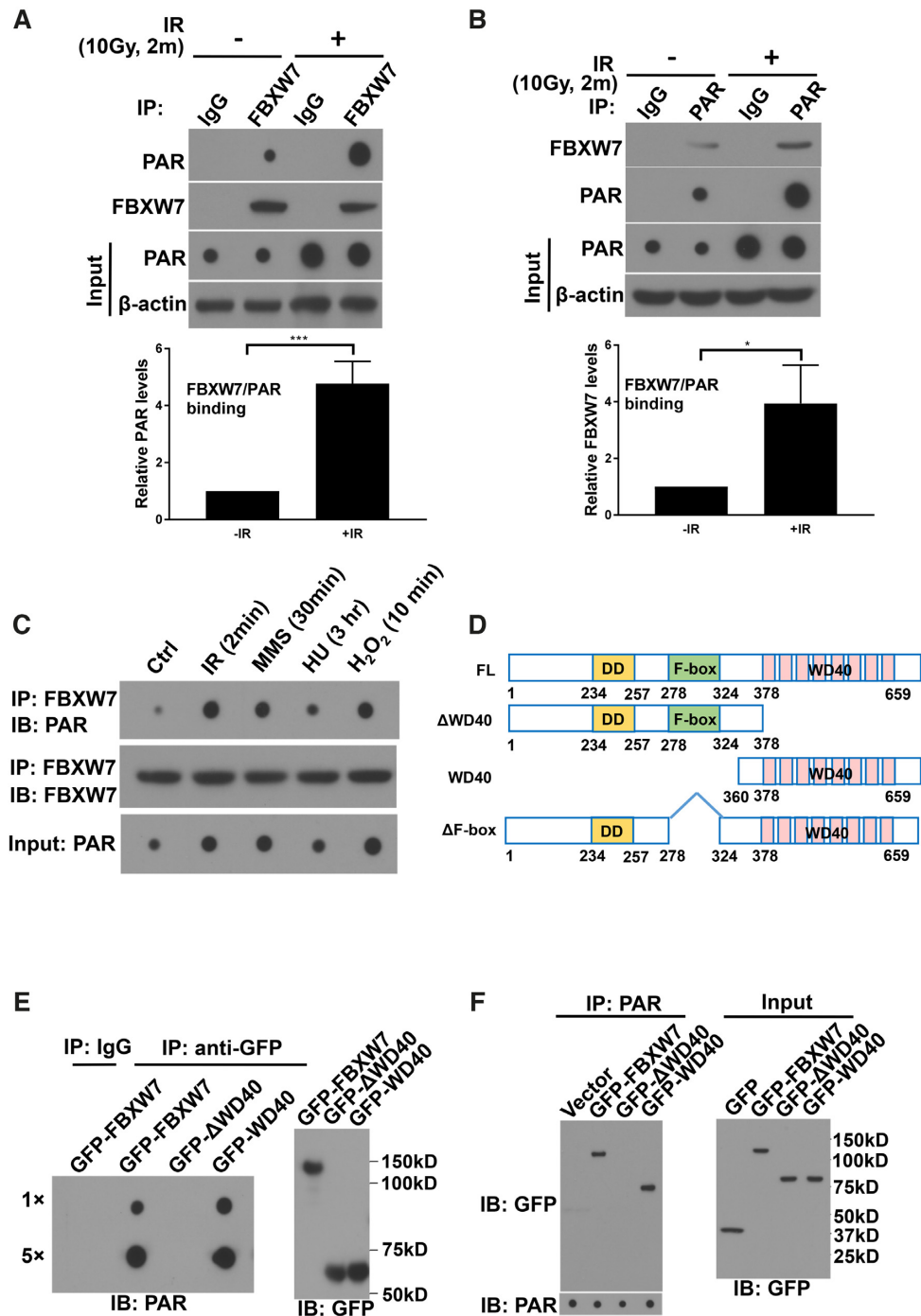
Figure 2. The WD40 domain of FBXW7 binds PAR in vivo in response to radiation-induced DNA damage. (**A** and **B**) MiaPaCa-2 cells were treated with or without 10 Gy of IR. Cells were lysed at 2 min after IR, and endogenous FBXW7 or PAR were immunoprecipitated with the indicated antibodies. Input or immunoprecipitated samples were analyzed by dot blotting (anti-PAR) or western blotting (anti-FBXW7). Data are from representative experiments (upper) or are the mean quantitated values of PAR or FBXW7 (normalized to control) from 3 independent experiments with statistically significant differences indicated (*$P < 0.05$; ***$P < 0.001$) (lower). (**C**) MiaPaCa-2 cells were treated with IR (10 Gy), Methyl methanesulfonate (MMS, 5μM), Hydroxyurea (HU, 2μM), or hydrogen peroxide (H_2O_2, 50 μM) respectively. Cells were harvested at the indicated times and endogenous FBXW7 was immunoprecipitated with anti-FBXW7 antibody and PAR was detected by dot blot with the anti-PAR. (**D**) FBXW7 deletion mutants used in this study with either an HA or GFP tag. (**E**) The WD40 domain of FBXW7 is essential for interaction with PAR *in vivo*. GFP-FBXW7 (full length), GFP-ΔWD40, and GFP-WD40 were transfected into MiaPaCa-2 cells. At 48 h after transfection, cells were lysed at 2 min post-IR (10 Gy). For immunoprecipitation of GFP-fusion full length FBXW7 and deletion mutants, cells were incubated with GFP antibody and the immunoprecipitates and input with 1× concentration or a 5× concentration were analyzed with PAR antibody. (**F**) A reciprocal co-IP assay to detect the interaction of PAR and the WD40 domain of FBXW7.
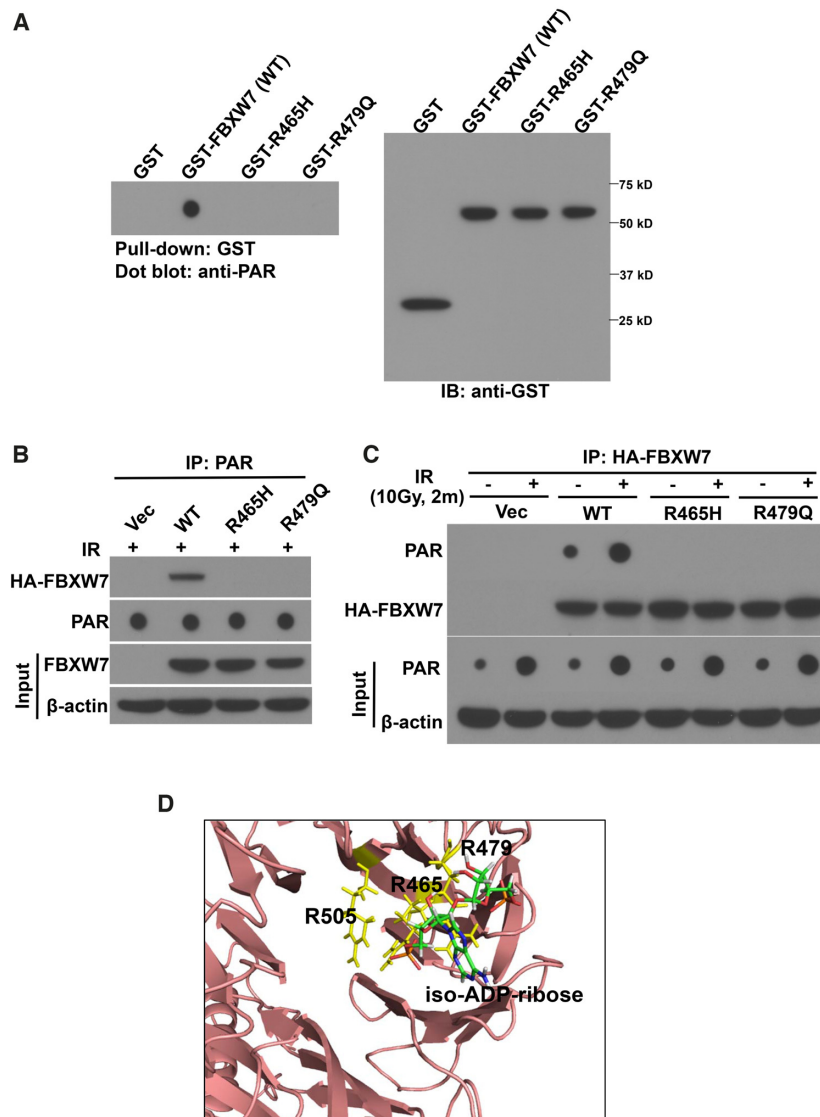
Figure 3. Cancer-associated mutations in the FBXW7-WD40 domain disrupt PAR binding. (**A**) Mutations of conserved residues (R465H, R479Q) in the WD40 domains of FBXW7 abolish the PAR binding *in vitro*. (**B**) HA-tagged WT FBXW7 and the indicated mutants (R465H, R479Q) were expressed in MiaPaCa-2 cells, cells were incubated with PAR antibody and WT and mutant FBXW7 were analyzed with anti-HA antibody. (**C**) The R465H and R479Q WD40 domain mutants of FBXW7 did not bind to PAR in a reciprocal co-IP assay. (**D**) FBXW7 WD40 is shown in the cartoon in salmon color; key residues of FBXW7 WD40 for interaction with iso-ADP-ribose are shown as yellow sticks. For docking simulation, FBXW7 was preprocessed with protons added according to pH 7.0. Then Glide module from Schrodinger software was used for iso-ADP-ribose docking into binding sites (56). While docking, key residues found important for PAR interaction with FBXW7 WD40 were assigned at the center of the enclosing box and SP (standard precision) mode was used. The top 20 dockings were analyzed and the one similar to the phospho-peptide binding is shown.

FBXW7 WD40-PAR binding is dependent on PARP1-mediated PAR synthesis

Given that PARP1/2 catalyzes the synthesis of PAR at DNA damage sites, the ability of PARP1/2 inhibitors, olaparib and veliparib to reduce FBXW7-PAR interaction was assessed. Treatment of cells with olaparib or veliparib inhibited the association between endogenous or overexpressed FBXW7 and PAR (Figure 4A and Supplementary Figure S4A). This result was further verified by reciprocal immunoprecipitation assays that demonstrated the ability of PARP inhibitors to reduce PAR levels and therefore also reduce the interaction between FBXW7 and PAR (Figure 4B). To discern the contributions of PARP1 and PARP2

to the FBXW7-PAR interaction in response to radiation, PARP1 or PARP2 were individually silenced. While the interaction between FBXW7 and PAR was unaffected in response to PARP2 siRNA, PARP1 silencing caused a significant reduction in the interaction of FBXW7 with PAR, a result that is likely due to the decreased levels of PAR (Figure 4C, D and Supplementary Figure S4B). To rule out that the increased association of FBXW7 with PAR is due to covalent PAR-modification of FBXW7 itself, FBXW7 was immunoprecipitated from cells under denaturing conditions (1% SDS) and analyzed for the presence of covalently bound PAR by western blotting. Consistent with a non-covalent interaction between FBXW7 and PAR, denat-
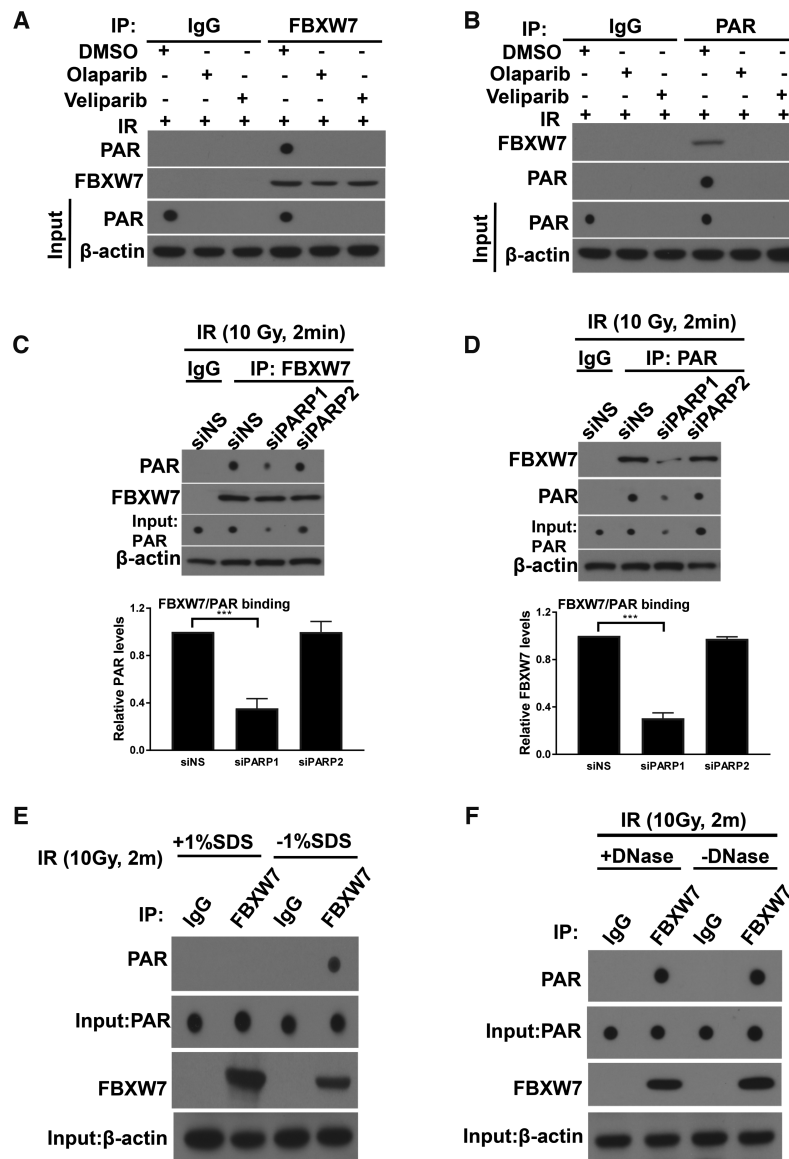
Figure 4. FBXW7 binds to PAR in vivo in a PARP1-dependent manner. (A and B) The *in vivo* interaction between FBXW7 and PAR after IR treatment was examined by co-IP (**A**) and reciprocal co-IP (**B**) in the presence or absence of PARP inhibitors, olaparib (1 μM) or veliparib (1 μM). IgG was included as the IP control. (**C** and **D**) The *in vivo* interaction of FBXW7 and PAR is impaired by depletion of PARP1. MiaPaCa-2 cells treated with PARP1, PARP2, or non-specific (NS) siRNAs were lysed and incubated with FBXW7 (C) or PAR (D) antibody and blotted with the indicated antibodies. The whole-cell lysates were blotted and are shown as the input. Data are from representative experiments (upper) or are the mean ± SE levels of PAR (C) or FBXW7 (D) binding in the immunoprecipitated samples relative to siNS controls from three independent experiments with statistical significance indicated (lower; ***P < 0.001). (**E**) FBXW7 does not covalently bind PAR upon IR treatment. MiaPaCa-2 cell lysates were incubated with FBXW7 antibody or IgG control antibody in the presence or absence of 1% SDS. The inputs and immunoprecipitates were analyzed with the indicated antibodies. (**F**) The interaction of FBXW7 and PAR is independent of DNA. Treatment of DNase in the cell lysates was not able to abolish the interaction of FBXW7 and PAR *in vivo* by co-IP assay.

uration of the samples prevented the interaction between FBXW7 and PAR (Figure 4E). In addition, the association between FBXW7 and PAR was independent of DNA, since the interaction was intact in cell lysates treated with DNase I (Figure 4F).

The WD40 domain mediates the early recruitment of FBXW7 to DNA damage sites

FBXW7α is phosphorylated by ATM (Ser26) which promotes its accumulation at DNA damage sites (21). To dis-

cern the requirement for ATM in the early recruitment versus retention of FBXW7 at DNA damage, we measured the kinetics of GFP-FBXW7 localization to DNA damage. Consistent with our prior study, in ATM wild-type cells, FBXW7 localized and was retained at laser microirradiation-induced DNA damage sites (Supplementary Figure. S5A, upper panel). In ATM null cells, however, while FBXW7 was quickly recruited to DNA damage sites (1–2 min), it was not retained there, as evidenced by the diminished signal at later time points (5–15 min; lower panel).

Consistent with these findings, mutation of the ATM phosphorylation site Ser26 to alanine (S26A) in FBXW7 caused dissociation of FBXW7 from DNA damage sites following its initial recruitment with kinetics similar to those observed in the ATM null cells (Supplementary Figure S5B). Furthermore, localization of FBXW7 to DNA damage sites was not dependent on the FBXW7 substrate XRCC4 (Supplementary Figure S5C). These results demonstrate that the early recruitment of FBXW7 to DNA damage is independent of ATM and XRCC4 suggesting that early recruitment may be PAR dependent.

To determine the relative importance of the WD40 domain to the recruitment of FBXW7 to DNA damage, we assessed the localization kinetics of different GFP-labeled FBXW7 fragments including those containing the N-terminus (ΔWD40), C-terminus (WD40), and both the N- and C-termini but with the F-box deleted (ΔF-box) (Figure 2D). We found in the absence of DNA damage that both the ΔWD40 and ΔF-box fragments were localized in the nucleoplasm similar to full length FBXW7, while the WD40 domain was predominantly in the nucleolus (Figure 5A). Consistent with the hypothesis that the WD40 domain is required for early localization of FBXW7 to damage sites, localization of the ΔWD40 fragment to DNA damage was delayed (Figure 5A, B). At later time points (10–15 min), ΔWD40 localized to DNA damage, a result consistent with ATM phosphorylation of Ser26 in the N-terminus of FBXW7 (21) promoting late recruitment and retention of FBXW7 at DNA damage sites. Despite the enrichment of WD40 in the nucleolus which is likely attributable to deletion of the nuclear localization sequence in the N-terminus (24), initial localization of the WD40 fragment to DNA damage was observable although it was not efficiently retained there (5–15 min), a finding consistent with rapid PAR synthesis and degradation at DNA damage sites (6). Furthermore, the ΔF-box fragment (Figure 5A) localized to the damage sites with kinetics similar to full length FBXW7, suggesting that FBXW7 binding to other SCF components is not required for localization. Collectively, these data demonstrate that the WD40 domain of FBXW7 is required for its early recruitment to DNA damage sites while the ATM phosphorylation site within the N-terminus is required for retention at DNA damage sites.

Given that mutation of arginine residues in the WD40 domain of FBXW7 abolished the interaction between FBXW7 and PAR, we next assessed whether these mutations also impaired the ability of FBXW7 to localize to DNA damage. In contrast to wild type FBXW7, the WD40 domain mutants R465H and R479Q were not efficiently recruited to laser microirradiation-induced DNA damage sites (Figure 5C, D). Furthermore, similar to ΔWD40, late recruitment of these mutants to DNA damage sites was less efficient than that of wild type FBXW7 (Figure 5C, D). Finally, we found that R465H and R479Q mutants have reduced FBXW7 phosphorylation relative to wild type FBXW7 in response to radiation (Figure 5E). Thus, although R465H and R479Q mutants have an intact Ser26 site which promotes late recruitment, ATM phosphorylation of the FBXW7 mutants is compromised in the absence of initial PAR-dependent recruitment. Collectively, these results demonstrate that the WD40 domain is impor-

tant for the early recruitment of FBXW7 to DNA damage sites, and that mutations which impair this early enrichment subsequently impede ATM-dependent phosphorylation and FBXW7 retention at DNA damage sites.

Early recruitment of FBXW7 to DNA damage is mediated by PAR

To further investigate the involvement of PAR in the early recruitment of FBXW7 to DNA damage sites, PAR synthesis was blocked with the PARP inhibitors olaparib or veliparib (37). The early recruitment of FBXW7 to DNA damage sites was inhibited by olaparib or veliparib, as evidenced by limited recruitment occurring only at later time points (Figure 6A, B). In response to ATM inhibitor (KU55933), while early recruitment was observed, late recruitment and retention of FBXW7 were impaired. When cells were treated with the combination of both PARP and ATM inhibitors, both early and late recruitment were abrogated (Figure 6A, B), supporting the notion that PAR and ATM are two consecutive signals required for efficient localization and retention of FBXW7 at DNA damage sites.

To further discern the role of PAR in the recruitment of FBXW7 to DNA damage, localization of the FBXW7-WD40 fragment, which lacks an ATM phosphorylation site, was assessed in response to inhibition of PAR synthesis or degradation. In response to treatment with olaparib or veliparib to inhibit PAR synthesis, FBXW7 WD40 was not recruited to DNA damage sites (Supplementary Figure S6A, B). Furthermore, since PAR is quickly hydrolyzed by poly(ADP-ribose) glycohydrolase (PARG) (34,38), we assessed the effect of the PARG inhibitor (gallotannin, GLTN) on the localization kinetics of the WD40 domain. Consistent with the ability of gallotannin to block PAR degradation, the WD40 domain of FBXW7 was retained at DNA damage sites despite the absence of the ATM-phosphorylation residue (S26) in this WD40 fragment (Supplementary Figure S6A, B). In line with this observation, we found a persistent interaction between FBXW7 and PAR upon gallotannin treatment (Supplementary Figure S6C). Furthermore, consistent with the reduction in PAR and FBXW7-PAR interactions in response to PARP1 silencing (Figure 4C, D), silencing PARP1 (but not PARP2) also blocked the early recruitment of FBXW7 to DNA damage sites (Figure 6C, D). Taken together, these results indicate that sequential and coordinated signaling of PARP1, PARG and ATM is required for efficient localization and retention of FBXW7 at DNA damage sites.

PAR-mediated early recruitment of FBXW7 regulates DNA damage repair

On the basis of our prior study which demonstrated that FBXW7 ubiquitinates XRCC4 to promote NHEJ following radiation-induced DNA damage (21), we performed an *in vivo* ubiquitination assay to determine whether this activity of FBXW7 was dependent on PAR at DNA damage sites. We found that inhibition of PARP (olaparib, veliparib) or ATM activity (KU55933) significantly impaired polyubiquitination of XRCC4 by FBXW7 (Figure 7A). These effects were comparable to those of pevonedistat (MLN4924), a
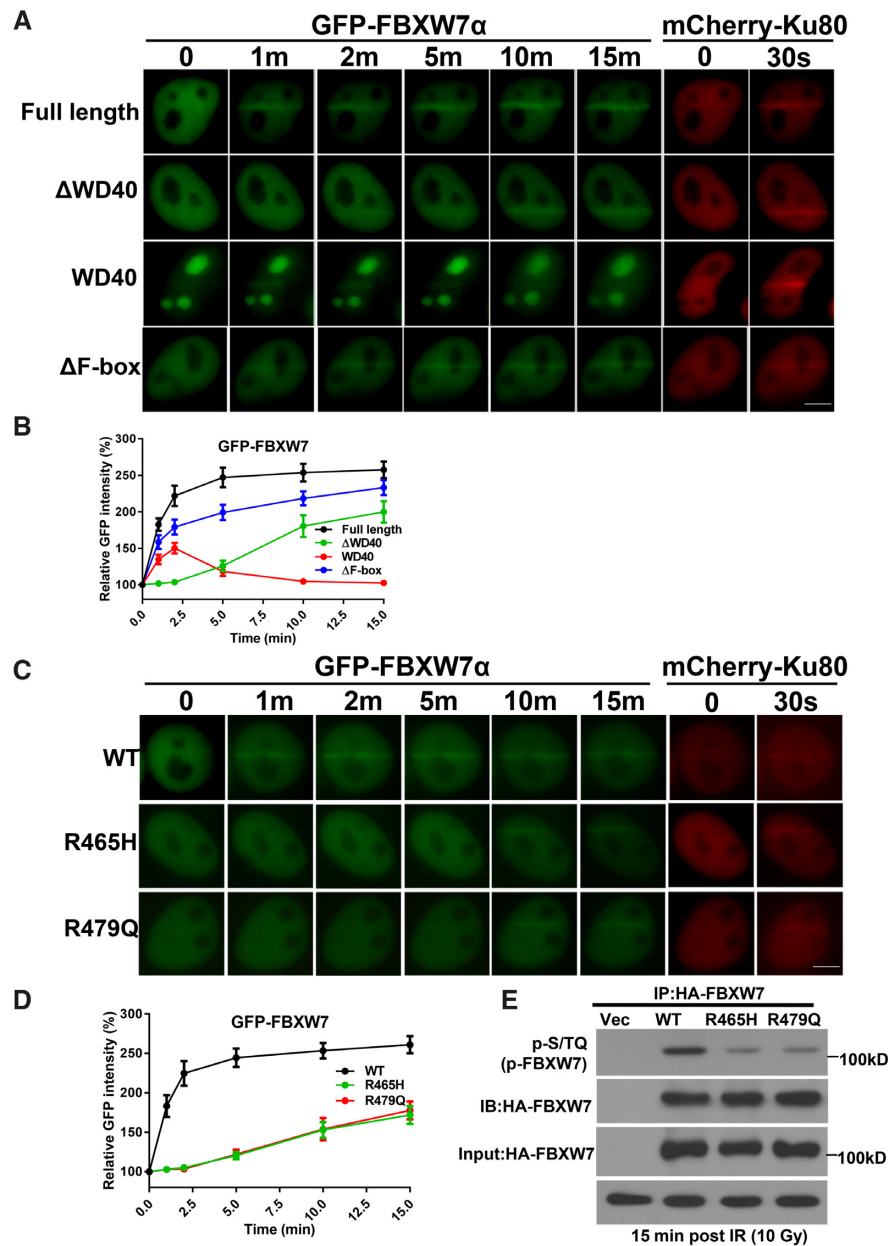
Figure 5. The WD40 domain of FBXW7 mediates early recruitment to DNA damage. (**A, B**) GFP-FBXW7 (full length and different deletion mutants) localization to microIR-induced DNA damage sites was monitored and quantified for up to 15min post-microIR in MiaPaCa-2 cells. Data are from a representative experiment (A) or are plotted as the percentage increase in fluorescence (arbitrary units) at the site of microIR and are the mean ± SE of 15 cells acquired from three independent experiments for each condition (B). mCherry-Ku80 was used as a positive control to indicate DNA damage upon microIR. (**C, D**) The relocation kinetics of FBXW7 WT and mutants to DNA damage sites. GFP-tagged WT, R465H and R479Q FBXW7 were expressed in MiaPaCa-2 cells, and the relocation kinetics were monitored over a period of 15 min following microIR. Data are from a representative experiment (C) or are the mean ± SE percentage increase in fluorescence of 15 cells acquired from three independent experiments for each condition (D). (Scale bar: 10 μm) (**E**) Radiation-induced phosphorylation of FBXW7 is reduced in the R465H and R479Q mutants. MiaPaCa-2 cells transfected with empty vector, HA-tagged FBXW7 WT or two mutants were irradiated (10 Gy) and collected at 15 min after radiation. The cell lysates were immunoprecipitated with anti-HA antibody and immunoblotted with anti-pS/TQ antibody to detect phosphorylation of FBXW7.

drug which inhibits cullin-RING ligase activity by preventing cullin neddylation (39) and thus blocks FBXW7 ubiquitination of XRCC4. These results suggest that the early recruitment and retention of FBXW7 to DNA damage sites by PAR and ATM, respectively, are required for subsequent ubiquitination of XRCC4.

To further support the concept that PAR is necessary for the recruitment of FBXW7 to DSBs and the subsequent binding and ubiquitination of XRCC4, we assessed the ability of cancer-derived FBXW7 mutations to interact with and ubiquitinate XRCC4. In contrast to the wild type WD40 domain, R465H and R479Q mutants failed to
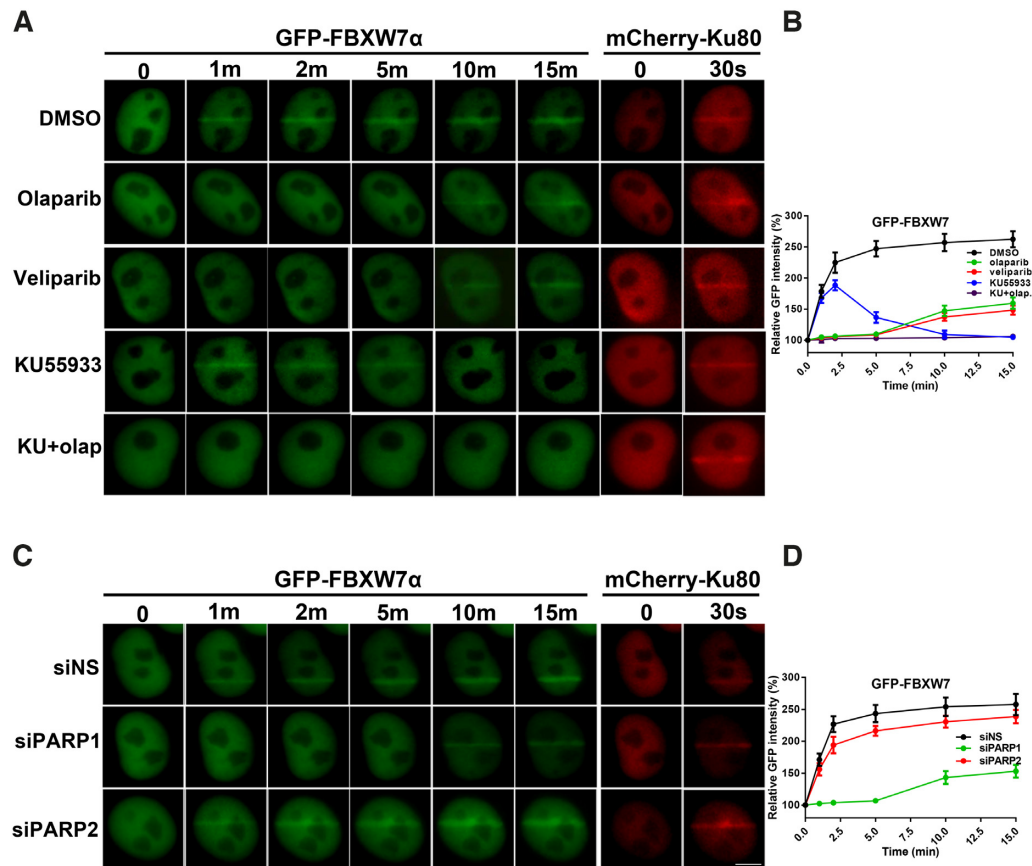
Figure 6. Rapid recruitment of FBXW7 to DNA damage is mediated by PARP1 and PAR. (**A**, **B**) The effect of PARPi and ATMi treatment on the recruitment of GFP-FBXW7 to DNA damage sites. GFP-FBXW7 was expressed in MiaPaCa-2 cells pretreated by PARPi (1 μM) and/or ATMi (10 μM) 1 h before microIR. The relocation of GFP-FBXW7 was examined in a time course (0–15 min) following microIR. (**C**, **D**) Depletion of PARP1, but not PARP2, abolishes the early recruitment of GFP-FBXW7 to DNA damage sites. GFP-FBXW7 was expressed in MiaPaCa-2 cells with depletion of PARP1 or PARP2. The recruitment of GFP-FBXW7 to DNA lesions was examined at different indicated time points. Data are from representative experiments (A, C) or are the mean ± SE normalized value ($n = 15$, 5 cells/condition from three independent biological replicates) (B, D) (scale bar: 10 μm).

bind XRCC4 and displayed reduced ability to ubiquitinate XRCC4 (Supplementary Figure S7A, B).

To assess the functional consequences of these mutants, NHEJ activity was assessed in cells stably expressing either wild type or FBXW7 mutants. Consistent with our previous findings, FBXW7 null cells (vector control) displayed reduced NHEJ activity that was rescued by wild type FBXW7 (Figure 7B) (21). Importantly, FBXW7 WD40 domain mutants had a complete loss of NHEJ activity, a result that was paralleled by decreased survival in the FBXW7 mutants either in the presence and absence of radiation without any effect on homologous recombination (Supplemental Figures S7C and D). Moreover, PARP inhibition by olaparib significantly inhibited the NHEJ activity in the cells with wild type FBXW7, while the effect of olaparib on the NHEJ activities in the FBXW7 mutant cells was marginal (Figure 7B). Given that NHEJ is a rapid and predominant DSB repair mechanism, we assessed DSB repair as a function of FBXW7 mutation or olaparib treatment. Using a neutral comet assay, we found that expression of wild type FBXW7 facilitated DNA repair relative to vector control FBXW7 null cells (Figure 7C, D). Furthermore, repair of radiation-induced DSBs was significantly impaired

at early time points (10-20 minutes) in cells expressing mutant FBXW7 relative to wild type FBXW7. As expected, olaparib also delayed the resolution of radiation-induced DSBs to an extent comparable to that of FBXW7 mutation. These findings were further supported by the persistence of radiation-induced γH2AX in FBXW7 null cells or in response to olaparib (Supplementary Figure S7E, F). Importantly, olaparib had a greater effect in FBXW7 wild type than in FBXW7 null cells (Supplementary Figure S7E, F) further supporting the importance of FBXW7 interactions with PAR in DSB repair.

DISCUSSION

In this study, we have found that the WD40 domain in FBXW7 (and DDB2) is a novel PAR binding domain that facilitates rapid recruitment of FBXW7 to DNA damage sites. Functionally, the rapid recruitment of FBXW7 to DNA damage sites promotes ATM-dependent phosphorylation and retention at damage sites, XRCC4 ubiquitination, and activation of NHEJ. Importantly, this study demonstrates that the binding of FBXW7 to PAR and in turn the functional consequences are abrogated by both PARP inhibitors as well as FBXW7 WD40 domain mu-
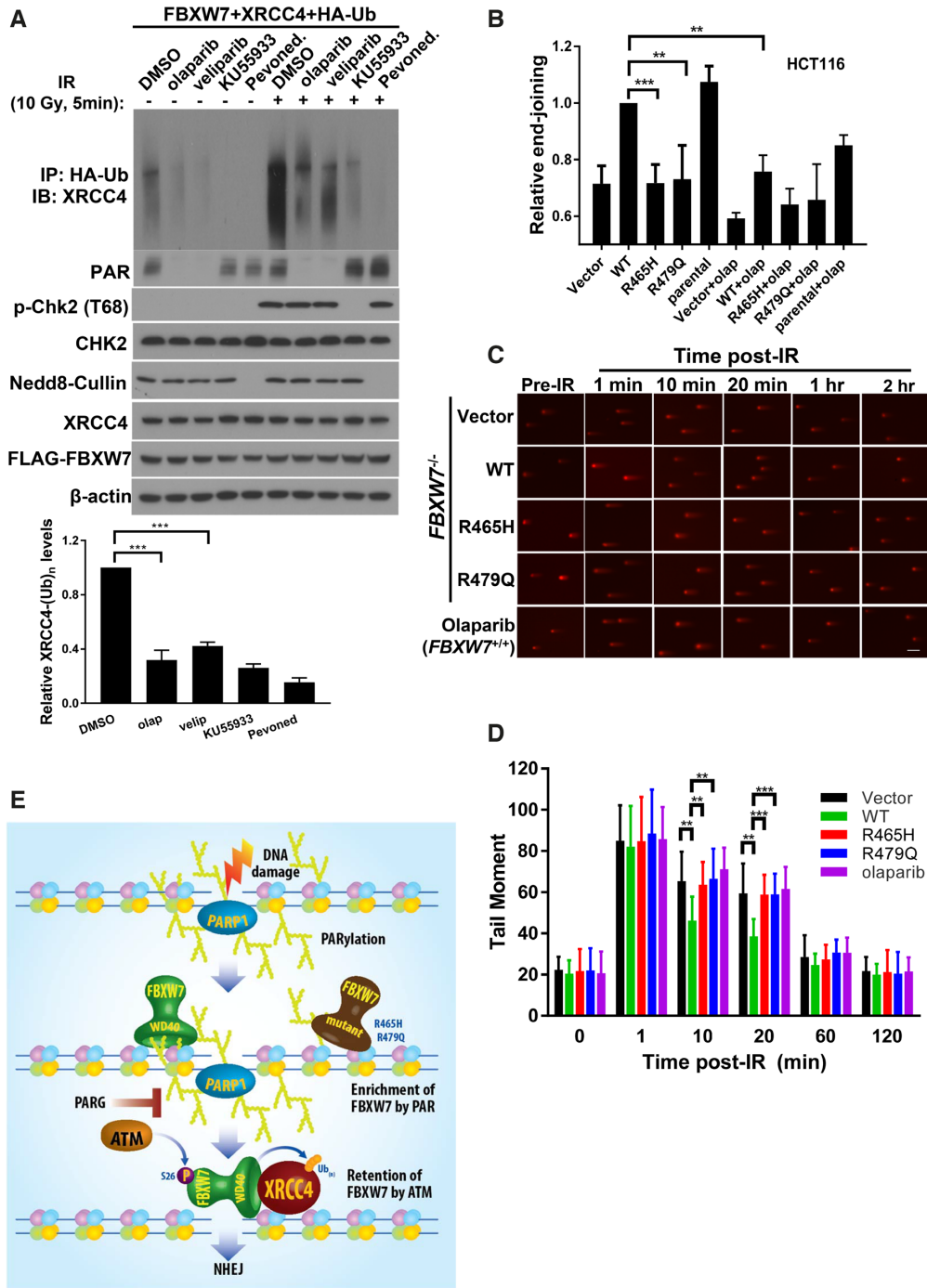
Figure 7. The interaction between FBXW7 and PAR facilitates XRCC4 ubiquitination and early DNA damage repair. (**A**) Pharmacological inhibition of PARP, ATM or SCF-FBXW7 inhibits XRCC4 ubiquitination at 5 min post-IR treatment. MiaPaCa-2 cells transfected with the indicated constructs were pretreated with inhibitors (1 h) and irradiated (10 Gy). XRCC4 ubiquitination was examined by IP with HA antibody, followed by IB for the XRCC4 protein. Input was blotted with indicated antibodies. Data are from a representative experiment (upper) or are the mean ± SE levels of polyubiquitinated XRCC4 in the immunoprecipitated samples normalized to control from three independent experiments with statistical significance indicated (***$P <$ 0.001). (**B**) NHEJ activity was assessed in FBXW7 isogenic HCT116 cells stably expressing FBXW7 WT or R465H or R479Q mutants with or without 1 µM olaparib. Data are the mean ± SE of three independent experiments. (**C**) Representative microphotographs of comet assay from cells at indicated time points following 5 Gy of IR. HCT116 FBXW7 isogenic cells were reconstituted with empty vector, WT FBXW7, or the indicated FBXW7 mutants. HCT116 parental cells treated with olaparib were used as a positive control. Scale bar, 100 µm. (**D**) Comet tail moments were analyzed from at least 100 cells for each experimental condition and are expressed as the mean ± SE from two independent experiments with statistical significance indicated (*$P <$ 0.05, ***P $<$ 0.001, ****$P <$ 0.0001). (**E**) A model of PAR-dependent recruitment of FBXW7 to DNA damage sites. Upon DNA damage, PARP1 accounts for the majority of protein PARylation. The WD40 domain of FBXW7 binds to PAR and mediates the early recruitment of FBXW7 to DNA damage sites where it is retained by ATM-mediated phosphorylation at S26 following PAR degradation by PARG. At DNA damage sites FBXW7 ubiquitinates XRCC4 to promote NHEJ. Cancer-associated mutations in the FBXW7 WD40 domain (at R479H or R465Q) disrupt the interaction with PAR subsequently leading to impaired XRCC4 ubiquitination and NHEJ.

tations. Given the prevalence of these FBXW7 WD40 mutations in human cancers (25,40), our study reveals a novel DNA repair defect associated with mutations in the FBXW7 WD40 domain that likely contributes to the genomic instability and tumorigenesis associated with FBXW7 loss-of-function (41–43). Furthermore, the results of this study uncover a novel mechanism by which PARP1 inhibitors delay DNA repair by reducing localization of WD40 domains to PAR at DNA damage sites.

The PAR polymer, both linear and branched, is highly anionic as a result of the two negative charges associated with each ADP-ribosyl moiety (5). Proteomic studies have shown that PAR binds hundreds of proteins through both covalent and non-covalent interactions (11,12). Importantly, several non-covalent PAR-binding motifs have been characterized, many of which also bind to DNA, RNA, or phosphopeptides. For example, several DNA/RNA binding motifs interact with PAR, such as the RNA recognition motif (RRM), the OB-fold, PIN domains, and the C-terminal domain of p53 (8,9,44,45). Furthermore, FHA and BRCT domains which are generally characterized as phospho-Thr and phospho-Ser recognition motifs, respectively, are also PAR-binding domains (10). These FHA and BRCT domains recognize the phosphate groups in the iso-ADP-ribose (the linkage of PAR) and the ADP-ribose unit, respectively (10). These findings provide a rationale for the biochemical and functional results in this study demonstrating that the FBXW7 WD40 domain which facilitates the interaction with many ubiquitin-ligase substrates by recognizing phospho-Ser/Thr also serves as a PAR binding domain. Furthermore, the ability of the DDB2 WD40 to bind PAR is consistent with its characterized function in binding damaged DNA (26), a feature that common in other PAR binding motifs.

In response to DNA damage, PAR is synthesized within seconds on PARP itself, on histones, as well as on other chromatin-associated proteins at DNA damage sites (46,47). ADP-ribosylation of PARP1 and presumably histones promotes the recruitment of many DNA repair proteins which contain poly(ADP-ribose) "reader" domains that are required for lesion processing and repair. Given that rapid relocation of FBXW7 to DNA lesions has been observed in this study, it is likely that PARylated PARP1 as well as histones plays an important role in mediating the recruitment of FBXW7 WD40 domains to DNA damage sites. It will be in important in future studies to define the relative contribution of PARylated substrates such as PARP1, PARP2, or various histones to the recruitment of FBXW7 to DNA damage sites.

The WD40 domain is a prominent characteristic of a large family of proteins that mediate protein-protein interactions (48,49). The low level of sequence conservation among different WD40 domain proteins, however, implies multiple modes of interactions. This concept is consistent with our finding that of the four DNA repair-related WD40 domain proteins investigated in this study, only FBXW7 and DDB2 were found to interact with PAR. While the unique features of these WD40 domains that mediate PAR binding are unknown, there are some potentially relevant known characteristics. FBXW7 contains a stretch of eight WD40 repeats, which interact with nearly

40 substrates. Crystallographic studies have demonstrated that the WD40 repeats consist of an eight-bladed barrel-shaped beta-propeller tertiary structure with relatively defined phospho-degron binding pockets (50). In addition, key arginine residues within repeats 3 and 4 are required for the contacts with phosphorylated substrates (24,50). Our biochemical and computational modeling data demonstrate that these arginine residues are also critical for the interaction of FBXW7 WD40 with PAR (Figure 3 and Supplementary Figure S3C-D). On the other hand, DDB2 is a 7-repeat WD40 protein in the DDB1–DDB2–CUL4A–RBX1 complex (Cullin4^{DDB}). The positively charged top surface of the DDB2 β-propeller interacts with damaged DNA, and several basic residues bind the DNA phosphodiester backbone (26). Although it has been recently shown that DDB2 associates with both PARP1 and PAR in the vicinity of UV-damaged chromatin (32), our findings demonstrate that the WD40 domain of DDB2 is responsible for the PAR binding. Therefore, the common feature of the WD40 domains of FBXW7 and DDB2 affinities to PAR is most likely due to electrostatic interactions between positively charged residues and the negatively charged PAR chains.

PARP and PAR have important functions in major DNA damage response pathways including both SSB and DSB repair as well as DNA synthesis underscoring their broader function in maintaining genome stability and thus suppressing tumorigenesis (51). The finding in this study that loss-of-function mutations in the FBXW7 WD40 domain disrupt binding with PAR (Figure 3) is consistent with the genomic instability (41) and tumorigenesis (52) associated with FBXW7 mutation or deletion, as well as the prevalence of FBXW7 WD40 domain mutations in human cancers (25,40). Although this is a unique mechanistic finding relevant to FBXW7 WD40, it is not the only example of mutations in tumor suppressors that disrupt PAR binding. For example, cancer-associated mutations in the BRCT domain of BARD1 (C645R and V695L) impair the interaction between BARD1 and PAR (53). This inability of BARD1 to bind PAR has important functional consequences in that it delays recruitment of BRCA1 to DNA damage sites and reduces the efficacy of PARP inhibitors. Cancer-associated mutations in the OB-fold domain of BRCA2 (R2659K, G2724A and S2988G) also disrupt binding with PAR and as a result, inhibit the recruitment of EXO1 and the early end resection steps of HR (54). In addition, consistent with these findings, mutations in the WD40 domain of DDB2 occur in human cancers suggesting an inability of these mutants to bind PAR (55). Taken together, these data demonstrate an association between cancer and the DNA repair defects caused by mutations in PAR binding domains.

In summary, our results support the following model: Upon DNA damage, PAR is rapidly synthesized and binds to the WD40 domain of FBXW7 to facilitate the rapid recruitment of FBXW7 to DNA damage sites. Subsequently, ATM-mediated FBXW7 phosphorylation at S26 facilitates the retention of FBXW7 at DNA damage sites following PAR degradation by PARG, leading to polyubiquitylation of XRCC4 via K63 linkage to set up a platform for effective recruitment of Ku70/80 for NHEJ repair. Cancer-associated arginine mutations in the FBXW7 WD40 do-

main or PARP inhibitor treatment impairs the interaction between the FBXW7 WD40 domain and PAR, resulting in delayed and reduced FBXW7 localization to DNA damage sites and inhibition of NHEJ (Figure 7E).

SUPPLEMENTARY DATA

Supplementary Data are available at NAR Online.

ACKNOWLEDGEMENTS

FUNDING

REFERENCES

1. Leung,A.K. (2014) Poly(ADP-ribose): an organizer of cellular architecture. *J. Cell Biol.*, **205**, 613–619.
2. Bai,P. (2015) Biology of poly(ADP-ribose) polymerases: the factotums of cell maintenance. *Mol. Cell*, **58**, 947–958.
3. Ray Chaudhuri,A. and Nussenzweig,A. (2017) The multifaceted roles of PARP1 in DNA repair and chromatin remodelling. *Nat. Rev. Mol. Cell Biol.*, **18**, 610–621.
4. Wei,H. and Yu,X. (2016) Functions of PARylation in DNA damage repair pathways. *Genomics Proteomics Bioinformatics*, **14**, 131–139.
5. Alvarez-Gonzalez,R. and Jacobson,M.K. (1987) Characterization of polymers of adenosine diphosphate ribose generated in vitro and in vivo. *Biochemistry*, **26**, 3218–3224.
6. Teloni,F. and Altmeyer,M. (2016) Readers of poly(ADP-ribose): designed to be fit for purpose. *Nucleic Acids Res.*, **44**, 993–1006.
7. Barkauskaite,E., Jankevicius,G., Ladurner,A.G., Ahel,I. and Timinszky,G. (2013) The recognition and removal of cellular poly(ADP-ribose) signals. *FEBS J.*, **280**, 3491–3507.
8. Zhang,F., Shi,J., Chen,S.H., Bian,C. and Yu,X. (2015) The PIN domain of EXO1 recognizes poly(ADP-ribose) in DNA damage response. *Nucleic Acids Res.*, **43**, 10782–10794.
9. Zhang,F., Chen,Y., Li,M. and Yu,X. (2014) The oligonucleotide/oligosaccharide-binding fold motif is a poly(ADP-ribose)-binding domain that mediates DNA damage response. *Proc. Natl. Acad. Sci. U.S.A.*, **111**, 7278–7283.
10. Li,M., Lu,L.Y., Yang,C.Y., Wang,S. and Yu,X. (2013) The FHA and BRCT domains recognize ADP-ribosylation during DNA damage response. *Genes Dev.*, **27**, 1752–1768.
11. Gagne,J.P., Isabelle,M., Lo,K.S., Bourassa,S., Hendzel,M.J., Dawson,V.L., Dawson,T.M. and Poirier,G.G. (2008) Proteome-wide identification of poly(ADP-ribose) binding proteins and poly(ADP-ribose)-associated protein complexes. *Nucleic Acids Res.*, **36**, 6959–6976.
12. Daniels,C.M., Ong,S.E. and Leung,A.K. (2015) The promise of proteomics for the study of ADP-Ribosylation. *Mol. Cell*, **58**, 911–924.
13. Schapira,M., Tyers,M., Torrent,M. and Arrowsmith,C.H. (2017) WD40 repeat domain proteins: a novel target class? *Nat. Rev. Drug Discov.*, **16**, 773–786.
14. Reinhardt,H.C. and Yaffe,M.B. (2013) Phospho-Ser/Thr-binding domains: navigating the cell cycle and DNA damage response. *Nat. Rev. Mol. Cell Biol.*, **14**, 563–580.
15. Yu,H. (2007) Cdc20: a WD40 activator for a cell cycle degradation machine. *Mol. Cell*, **27**, 3–16.
16. Park,J.Y., Zhang,F. and Andreassen,P.R. (2014) PALB2: the hub of a network of tumor suppressors involved in DNA damage responses. *Biochim. Biophys. Acta*, **1846**, 263–275.
17. Henriksson,S., Rassoolzadeh,H., Hedstrom,E., Coucoravas,C., Julner,A., Goldstein,M., Imreh,G., Zhivotovsky,B., Kastan,M.B., Helleday,T. *et al.* (2014) The scaffold protein WRAP53beta orchestrates the ubiquitin response critical for DNA double-strand break repair. *Genes Dev.*, **28**, 2726–2738.
18. Silverman,J.S., Skaar,J.R. and Pagano,M. (2012) SCF ubiquitin ligases in the maintenance of genome stability. *Trends Biochem. Sci.*, **37**, 66–73.
19. Scrima,A., Fischer,E.S., Lingaraju,G.M., Bohm,K., Cavadini,S. and Thoma,N.H. (2011) Detecting UV-lesions in the genome: The modular CRL4 ubiquitin ligase does it best! *FEBS Lett.*, **585**, 2818–2825.
20. Ruthemann,P., Balbo Pogliano,C. and Naegeli,H. (2016) Global-genome nucleotide excision repair controlled by Ubiquitin/Sumo modifiers. *Front. Genet.*, **7**, 68.
21. Zhang,Q., Karnak,D., Tan,M., Lawrence,T.S., Morgan,M.A. and Sun,Y. (2016) FBXW7 facilitates nonhomologous End-Joining via K63-Linked Polyubiquitylation of XRCC4. *Mol. Cell*, **61**, 419–433.
22. Wang,J., Jo,U., Joo,S.Y. and Kim,H. (2016) FBW7 regulates DNA interstrand cross-link repair by modulating FAAP20 degradation. *Oncotarget*, **7**, 35724–35740.
23. Hong,X., Liu,W., Song,R., Shah,J.J., Feng,X., Tsang,C.K., Morgan,K.M., Bunting,S.F., Inuzuka,H., Zheng,X.F. *et al.* (2016) SOX9 is targeted for proteasomal degradation by the E3 ligase FBW7 in response to DNA damage. *Nucleic Acids Res.*, **44**, 8855–8869.
24. Welcker,M. and Clurman,B.E. (2008) FBW7 ubiquitin ligase: a tumour suppressor at the crossroads of cell division, growth and differentiation. *Nat. Rev. Cancer*, **8**, 83–93.
25. Davis,R.J., Welcker,M. and Clurman,B.E. (2014) Tumor suppression by the Fbw7 ubiquitin ligase: mechanisms and opportunities. *Cancer Cell*, **26**, 455–464.
26. Scrima,A., Konickova,R., Czyzewski,B.K., Kawasaki,Y., Jeffrey,P.D., Groisman,R., Nakatani,Y., Iwai,S., Pavletich,N.P. and Thoma,N.H. (2008) Structural basis of UV DNA-damage recognition by the DDB1-DDB2 complex. *Cell*, **135**, 1213–1223.
27. Eschenfeldt,W.H., Lucy,S., Millard,C.S., Joachimiak,A. and Mark,I.D. (2009) A family of LIC vectors for high-throughput cloning and purification of proteins. *Methods Mol. Biol.*, **498**, 105–115.
28. Olive,P.L. and Banath,J.P. (2006) The comet assay: a method to measure DNA damage in individual cells. *Nat. Protoc.*, **1**, 23–29.
29. Stoyanova,T., Roy,N., Kopanja,D., Raychaudhuri,P. and Bagchi,S. (2009) DDB2 (damaged-DNA binding protein 2) in nucleotide excision repair and DNA damage response. *Cell Cycle*, **8**, 4067–4071.
30. Liu,C., Wu,J., Paudyal,S.C., You,Z. and Yu,X. (2013) CHFR is important for the first wave of ubiquitination at DNA damage sites. *Nucleic Acids Res.*, **41**, 1698–1710.
31. Oberoi,J., Richards,M.W., Crumpler,S., Brown,N., Blagg,J. and Bayliss,R. (2010) Structural basis of poly(ADP-ribose) recognition by the multizinc binding domain of checkpoint with forkhead-associated and RING Domains (CHFR). *J. Biol. Chem.*, **285**, 39348–39358.
32. Robu,M., Shah,R.G., Petitclerc,N., Brind'Amour,J., Kandan-Kulangara,F. and Shah,G.M. (2013) Role of poly(ADP-ribose) polymerase-1 in the removal of UV-induced DNA lesions by nucleotide excision repair. *Proc. Natl. Acad. Sci. U.S.A.*, **110**, 1658–1663.
33. Pines,A., Vrouwe,M.G., Marteijn,J.A., Typas,D., Luijsterburg,M.S., Cansoy,M., Hensbergen,P., Deelder,A., de Groot,A., Matsumoto,S. *et al.* (2012) PARP1 promotes nucleotide excision repair through DDB2 stabilization and recruitment of ALC1. *J. Cell Biol.*, **199**, 235–249.
34. Kim,M.Y., Zhang,T. and Kraus,W.L. (2005) Poly(ADP-ribosyl)ation by PARP-1: 'PAR-laying' NAD+ into a nuclear signal. *Genes Dev.*, **19**, 1951–1967.
35. Akhoondi,S., Sun,D., von der Lehr,N., Apostolidou,S., Klotz,K., Maljukova,A., Cepeda,D., Fiegl,H., Dafou,D., Marth,C. *et al.* (2007) FBXW7/hCDC4 is a general tumor suppressor in human cancer. *Cancer Res.*, **67**, 9006–9012.

36. King,B., Trimarchi,T., Reavie,L., Xu,L., Mullenders,J., Ntziachristos,P., Aranda-Orgilles,B., Perez-Garcia,A., Shi,J., Vakoc,C. *et al.* (2013) The ubiquitin ligase FBXW7 modulates leukemia-initiating cell activity by regulating MYC stability. *Cell*, **153**, 1552–1566.

37. Parsels,L.A., Karnak,D., Parsels,J., Zhang,Q., Velez-Padilla,J., Reichert,Z., Wahl,D.R., Maybaum,J., O'Connor,M.J., Lawrence,T.S. *et al.* (2017) PARP1 trapping and DNA replication stress enhance radiosensitization with combined WEE1 and PARP inhibitors. *Mol. Cancer Res.*, **16**, 222–232.

38. Chand,S.N., Zarei,M., Schiewer,M.J., Kamath,A.R., Romeo,C., Lal,S., Cozzitorto,J.A., Nevler,A., Scolaro,L., Londin,E. *et al.* (2017) Posttranscriptional regulation of PARG mRNA by HuR facilitates DNA repair and resistance to PARP inhibitors. *Cancer Res.*, **77**, 5011–5025.

39. Soucy,T.A., Smith,P.G., Milhollen,M.A., Berger,A.J., Gavin,J.M., Adhikari,S., Brownell,J.E., Burke,K.E., Cardin,D.P., Critchley,S. *et al.* (2009) An inhibitor of NEDD8-activating enzyme as a new approach to treat cancer. *Nature*, **458**, 732–736.

40. Nakayama,K.I. and Nakayama,K. (2006) Ubiquitin ligases: cell-cycle control and cancer. *Nat. Rev. Cancer*, **6**, 369–381.

41. Rajagopalan,H., Jallepalli,P.V., Rago,C., Velculescu,V.E., Kinzler,K.W., Vogelstein,B. and Lengauer,C. (2004) Inactivation of hCDC4 can cause chromosomal instability. *Nature*, **428**, 77–81.

42. Grim,J.E., Knoblaugh,S.E., Guthrie,K.A., Hagar,A., Swanger,J., Hespelt,J., Delrow,J.J., Small,T., Grady,W.M., Nakayama,K.I. *et al.* (2012) Fbw7 and p53 cooperatively suppress advanced and chromosomally unstable intestinal cancer. *Mol. Cell Biol.*, **32**, 2160–2167.

43. Zhang,Q., Zhang,Y., Parsels,J.D., Lohse,I., Lawrence,T.S., Pasca di Magliano,M., Sun,Y. and Morgan,M.A. (2016) Fbxw7 deletion accelerates KrasG12D-Driven pancreatic tumorigenesis via yap accumulation. *Neoplasia*, **18**, 666–673.

44. Adamson,B., Smogorzewska,A., Sigoillot,F.D., King,R.W. and Elledge,S.J. (2012) A genome-wide homologous recombination screen identifies the RNA-binding protein RBMX as a component of the DNA-damage response. *Nat. Cell Biol.*, **14**, 318–328.

45. Fischbach,A., Kruger,A., Hampp,S., Assmann,G., Rank,L., Hufnagel,M., Stockl,M.T., Fischer,J.M.F., Veith,S., Rossatti,P. *et al.* (2018) The C-terminal domain of p53 orchestrates the interplay between non-covalent and covalent poly(ADP-ribosyl)ation of p53 by PARP1. *Nucleic Acids Res.*, **46**, 804–822.

46. D'Amours,D., Desnoyers,S., D'Silva,I. and Poirier,G.G. (1999) Poly(ADP-ribosyl)ation reactions in the regulation of nuclear functions. *Biochem. J.*, **342**, 249–268.

47. Alvarez-Gonzalez,R., Pacheco-Rodriguez,G. and Mendoza-Alvarez,H. (1994) Enzymology of ADP-ribose polymer synthesis. *Mol. Cell Biochem.*, **138**, 33–37.

48. Stirnimann,C.U., Petsalaki,E., Russell,R.B. and Muller,C.W. (2010) WD40 proteins propel cellular networks. *Trends Biochem. Sci.*, **35**, 565–574.

49. Xu,C. and Min,J. (2011) Structure and function of WD40 domain proteins. *Protein Cell*, **2**, 202–214.

50. Hao,B., Oehlmann,S., Sowa,M.E., Harper,J.W. and Pavletich,N.P. (2007) Structure of a Fbw7-Skp1-cyclin E complex: multisite-phosphorylated substrate recognition by SCF ubiquitin ligases. *Mol. Cell*, **26**, 131–143.

51. Tong,W.M., Cortes,U. and Wang,Z.Q. (2001) Poly(ADP-ribose) polymerase: a guardian angel protecting the genome and suppressing tumorigenesis. *Biochim. Biophys. Acta*, **1552**, 27–37.

52. Davis,H., Lewis,A., Behrens,A. and Tomlinson,I. (2014) Investigation of the atypical FBXW7 mutation spectrum in human tumours by conditional expression of a heterozygous propellor tip missense allele in the mouse intestines. *Gut*, **63**, 792–799.

53. Li,M. and Yu,X. (2013) Function of BRCA1 in the DNA damage response is mediated by ADP-ribosylation. *Cancer Cell*, **23**, 693–704.

54. Zhang,F., Shi,J., Bian,C. and Yu,X. (2015) Poly(ADP-Ribose) mediates the BRCA2-Dependent early DNA damage response. *Cell Rep.*, **13**, 678–689.

55. Oh,K.S., Emmert,S., Tamura,D., DiGiovanna,J.J. and Kraemer,K.H. (2011) Multiple skin cancers in adults with mutations in the XP-E (DDB2) DNA repair gene. *J. Invest. Dermatol.*, **131**, 785–788.

56. Friesner,R.A., Murphy,R.B., Repasky,M.P., Frye,L.L., Greenwood,J.R., Halgren,T.A., Sanschagrin,P.C. and Mainz,D.T. (2006) Extra precision glide: docking and scoring incorporating a model of hydrophobic enclosure for protein-ligand complexes. *J. Med. Chem.*, **49**, 6177–6196.